Chemical Engineering Journal 156 (2010) 313–320

Contents lists available at ScienceDirect

Chemical Engineering Journal

journal homepage: www.elsevier.com/locate/cej

Adsorption behavior of methylene blue onto titanate nanotubes

Lin Xiong[a,b], Ye Yang[c], Jiaxing Mai[a,b], Weiling Sun[a,b], Chaoying Zhang[c], Dapeng Wei[c], Qing Chen[c], Jinren Ni[a,b,*]

[a] Department of Environmental Engineering, Peking University, Beijing 100871, China
[b] The Key Laboratory of Water and Sediment Sciences, Ministry of Education, Beijing 100871, China
[c] Key Laboratory for the Physics and Chemistry of Nanodevices and Department of Electronics, Peking University, Beijing 100871, China

ARTICLE INFO

Article history:
Received 5 July 2009
Received in revised form 2 October 2009
Accepted 6 October 2009

Keywords:
Titanate nanotubes
Methylene blue
Adsorption kinetics
Isotherm
Mechanism

ABSTRACT

Calcined titanate nanotubes were synthesized with hydrothermal treatment of the commercial TiO_2 (Degussa P25) followed by calcination. The morphology and structures of as-prepared samples were investigated by transmission electron microscopy, X-ray diffraction and N_2 adsorption/desorption. The samples exhibited a tubular structure and a high surface area of 157.9 m^2/g. The adsorption of methylene blue onto calcined titanate nanotubes was studied. The adsorption kinetics was evaluated by the pseudo-first-order, pseudo-second-order and Weber's intraparticle diffusion model. The pseudo-second-order model was the best to describe the adsorption kinetics, and intraparticle diffusion was not the rate-limiting step. The equilibrium adsorption data were analyzed with three isotherm models (Langmuir model, Freundlich model and Temkin model). The best agreement was achieved by the Langmuir isotherm with correlation coefficient of 0.993, corresponding to maximum adsorption capacity of 133.33 mg/g. The adsorption mechanism was primarily attributed to chemical sorption involving the formation of methylene blue-calcined titanate nanotubes nanocomposite, associated with electrostatic attraction in the initial bulk diffusion.

1. Introduction

Titanium dioxide (TiO_2) has been widely used in heterogeneous photocatalysis due to its stable physico-chemical property and high photocatalytic activity. Nanotubular TiO_2-derived materials are particularly interesting since the discovery of carbon nanotubes in 1991 [1] and first fabrication of titania nanotubes in 1998 [2]. Among these, one-dimensional titanate nanotubes have attracted extensive attention for their particular morphology and unique physical and chemical properties. Such nanotubes can be synthesized via hydrothermal reaction between TiO_2 and NaOH [3–5]. The obtained nanotubes exhibit multi-walled scroll-type open-ended structures and have large internal and external surfaces and interlayer spaces. These peculiar microstructures make titanate nanotubes have great potential for applications as adsorbents and photocatalysts. Several works [6,7] have reported that titanate nanotubes with calcination post-treatment exhibit favorable photocatalytic activity.

It has been demonstrated that photocatalytic degradation rate depends on photocatalyst–pollutant molecule interaction and good adsorption of pollutant molecule can improve the efficiency of photocatalytic degradation [8–10]. The adsorption of pollutants is also of interest as it concerns other experimental studies, including photocatalyst surface modification [11], dye-sensitized photodegradation of organics [12], and so on. Obviously, it is of great importance to investigate the adsorption process of organic pollutants on the surface of titanate nanotubes to clarify the mechanism of photocatalytic reactions and facilitate the applications in contaminant destruction. Unfortunately, previous studies of titanate nanotubes focused on preparation, structure analysis and photocatalytic efficiency evaluation, and little attention were paid to identifying characteristic of organics adsorption onto titanate nanotubes. Furthermore, very few studies have been done with the focus on adsorption mechanism of organic pollutants on the surface of titanate nanotubes.

In the present work, titanate nanotubes (labeled as TNTs) were prepared by a hydrothermal reaction, whereafter the as-prepared nanotubes were calcined at a constant temperature. One of the familiar basic dyes, methylene blue (MB, Fig. 1), was employed as the model pollutant, and the adsorption of MB onto calcined titanate nanotubes (labeled as CTNTs) was systematically investigated. Specifically, the zeta potential at different pH for CTNTs suspension and attenuated total reflection-Fourier trans-

* Corresponding author at: Department of Environmental Engineering, Peking University, Beijing 100871, China. Tel.: +86 10 6275 1185; fax: +86 10 6275 6526.
E-mail address: nijinren@iee.pku.edu.cn (J. Ni).

1385-8947/$ – see front matter © 2009 Elsevier B.V. All rights reserved.
doi:10.1016/j.cej.2009.10.023

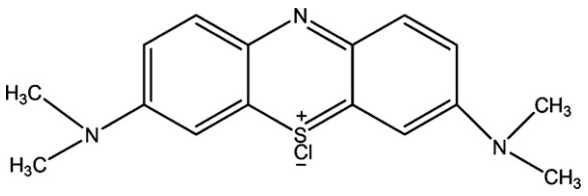

Fig. 1. Chemical structure of MB.

form infrared (ATR-FTIR) spectra of MB adsorption onto CTNTs were measured, and adsorption mechanism of MB onto CTNTs was discussed.

2. Materials and methods

2.1. Chemicals

MB (purity ≥98.5%, Beijing Chemical Reagents Company, Beijing, China) and TiO_2 (P25, Degussa, Frankfurt, Germany) were used as received. According to the manufacturer, Degussa P25 contains approximately 90% anatase and 10% rutile. A 3000 mg/L stock MB solution was first prepared in deionized water. Other chemicals such as sodium hydroxide and ethanol were purchased as analytical reagent. All the solutions used in the experiment were prepared with deionized water.

2.2. CTNTs preparation

Titanate nanotubes were synthesized by a hydrothermal process similar to that reported in Ref. [13]. In a typical synthesis, 0.3 g of Degussa P25 was added into a 10 M NaOH aqueous solution. After stirring for 24 h, the specimen was transferred into a sealed Teflon container statically heated at 130 °C for 72 h. Then the product was centrifugally separated at 4000 rpm and washed with ethanol at room temperature until the pH value of the supernatant dropped to about 7. The resulting powder was further dried at 80 °C for about 4 h in air. Finally, the samples were calcined at 400 °C in air for 2 h and CTNTs were obtained.

2.3. CTNTs characterization

Transmission electron microscopy (TEM) analysis was conducted with a FEI Tecnai G20 microscope operating at 200 kV. X-ray diffraction (XRD) patterns were obtained on a Rigaku Dmax/2400 X-ray diffractometer using Cu Kα radiation at a scan rate (2θ) of 8°/min (λ = 1.5418 Å). Specific surface area was measured through nitrogen adsorption and desorption at −196 °C using an ASAP 2010 adsorption apparatus (Micromeritics, USA). The Brunauer–Emmett–Teller (BET) surface area was determined in the relative pressure (P/P_0) range of 0.06–0.20. Nitrogen adsorption volume at the relative pressure of 0.99 was used to determine the pore volume and the average pore diameter. Prior to adsorption, the samples were degassed at 50 °C under a reduced pressure of 0.02 Torr.

2.4. Adsorption experiments

2.4.1. Kinetic experiments

All adsorption experiments were conducted at pH 7.0. For the adsorption kinetics, 0.0200 g of CTNTs was added to 40 mL of MB solution at the initial concentrations of 50 and 100 mg/L. The

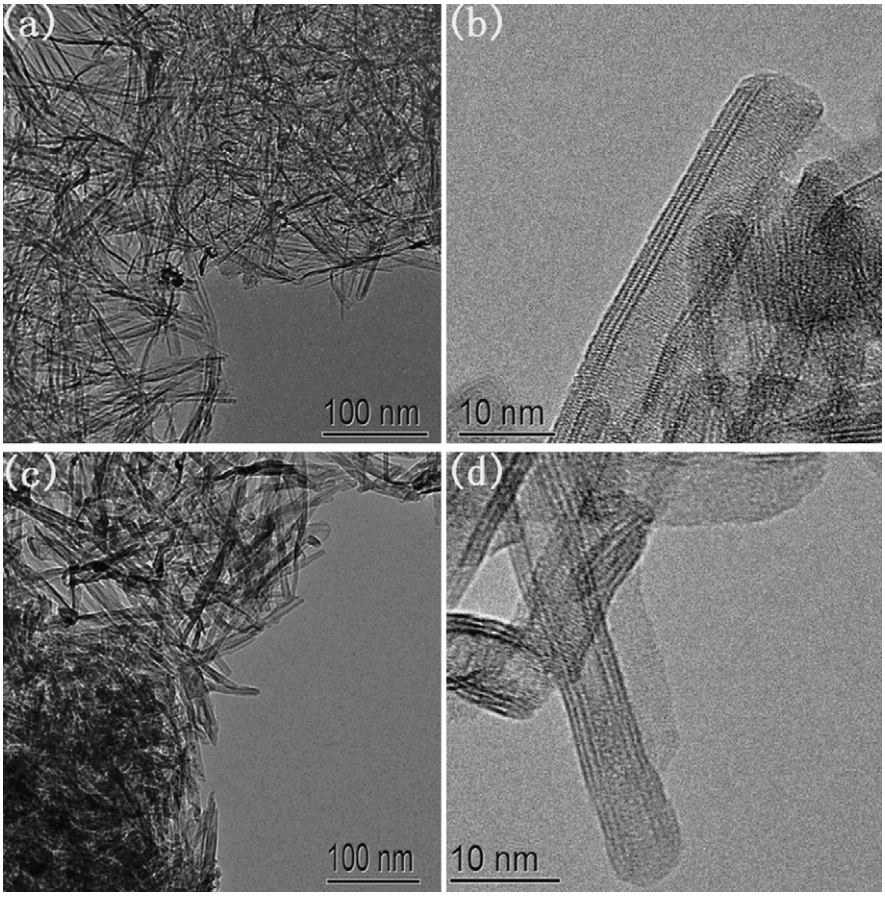

Fig. 2. TEM images of the samples. (a) TNTs, (b) HRTEM of the TNTs, (c) CTNTs, and (d) HRTEM of the CTNTs.

suspensions were left in conical flasks and agitated in an isothermal reciprocating shaker at 200 rpm and 25 °C. At appropriate time intervals, the aliquots were withdrawn from the solutions and centrifuged for 5 min at 4000 rpm to separate solid particles. The residual MB concentrations in the supernatant solutions were determined by absorbance measurement using UV–visible spectrophotometer (Specord 200, Analytik Jena AG, Germany) at its maximum absorption wavelength of 660 nm. It was then computed to MB concentration using standard calibration curve. The amount of MB adsorbed onto CTNTs at any time was computed by the difference between the initial MB concentration and the concentration at any time.

2.4.2. Equilibrium experiments

All batch equilibrium experiments were also carried out in conical flasks and rotated in the reciprocating shaker under the same conditions. To obtain the adsorption isotherm, CTNTs at a constant dose of 0.5 g/L were placed in MB solution of different concentrations (25–230 mg/L). Aliquots were taken from the flask at equilibrium, centrifuged, diluted and analyzed by UV–visible spectrophotometer to determine the initial and equilibrium MB concentrations in the solutions. The amount of MB adsorbed onto CTNTs at equilibrium was calculated by the difference between the initial and equilibrium MB concentrations.

3. Results and discussion

3.1. Morphology and structures of titanate nanotubes

Fig. 2 showed the TEM images of the as-prepared products. One can see that a large amount of randomly tangled nanotubes was obtained. The hollow and open-ended characteristics of the TNTs can be observed from the TEM micrograph as shown in Fig. 2(a). The HRTEM image (see Fig. 2(b)) indicated that the prepared nanotubes had uniform inner (ca. 4.5 nm) and outer diameters (ca. 9 nm) along the length. Moreover, the as-prepared nanotubes possessed multi-walled tubular structures and generally consisted of 3–4 layers, also as presented in Fig. 2(b). The interlayer distance, directly measured from HRTEM image, was ca. 0.75 nm. These results were in good consistency with the previous studies [3,14]. The morphology of CTNTs was illustrated in Fig. 2(c) and (d). It can be seen that calcination at 400 °C did not significantly change the morphology of the nanotubes, in which there were no differences between TNTs and CTNTs, except a slight decrease in inner and outer diameters. Since they had homogeneous multi-walled tubular structures and open ends, the CTNTs were expected to possess great potential in gaseous or liquid adsorption.

Fig. 3 presented the XRD patterns of the nanotubes before and after calcination. All the observed XRD peaks ($2\theta \approx 10°$, 24°, 28° and 48°) were assigned to TNTs, and the intense peak at about 10° was ascribed to interlayer space of TNTs, in accordance with the previous reports [3]. For comparison, the XRD pattern of TiO_2 was also presented. The XRD results indicated that the TiO_2 precursors were completely transformed to TNTs and no anatase or rutile phase appeared in the obtained nanotubes. Moreover, the XRD pattern of CTNTs was similar to that of TNTs, and all the characteristic peaks appeared, suggesting that calcination under experimental conditions did not damage the structure of the samples and the multi-walled tubular structures of CTNTs were maintained.

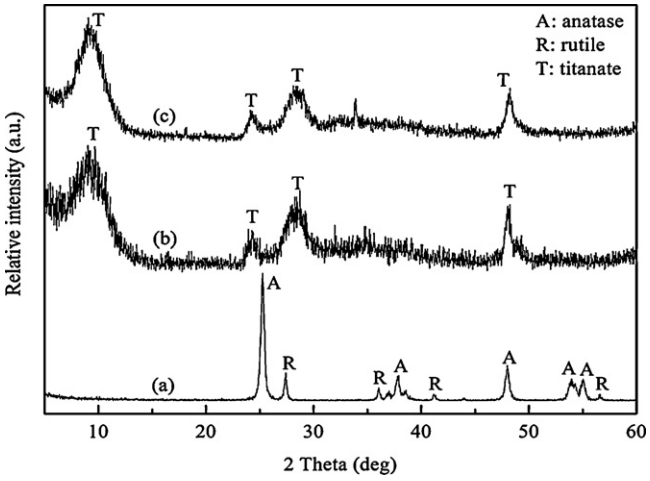

Fig. 3. XRD patterns of the samples. (a) TiO_2 (P25), (b) TNTs, and (c) CTNTs.

3.2. BET surface area and pore volume

According to nitrogen adsorption and desorption experiment, the textural parameters of samples were collected in Table 1. It can be seen that the synthesis of titanate nanotubes derived from TiO_2 (P25) result in an obvious increase in surface area and porosity. The measured BET surface area of CTNTs was 157.9 m^2/g. This was increased by a factor of 3.4 compared with Degussa P25 (46.9 m^2/g). However, the value of the surface area was found to be smaller than some previous reports [15,16]. This was presumably due to different synthesis conditions, including hydrothermal temperature, reaction time, post-treatment washing, etc. In addition, calcination post-treatment could also lead to the decrease in surface area [6,7]. In comparison, the surface area of the resulting CTNTs in this study was comparable to those similar reports. For instance, Yu and Zhou [7] fabricated titanate nanotubes with the surface area of 130.0 m^2/g after calcination at 400 °C. Lee et al. [17] showed that the nanotubes with higher surface area (ca. 190 m^2/g) can be obtained at the same calcination temperature. With respect to commercial TiO_2 (P25), the high specific surface area and porosity of as-synthesized CTNTs made it possible to adsorb pollutant molecules into the surface of the pores, thus favored photocatalytic degradation mediated with CTNTs.

3.3. Adsorption kinetics

To determine the time necessary to get access to equilibrium adsorption, the effect of contact time on adsorption of MB onto CTNTs was first studied at two different initial concentrations, viz. 50 and 100 mg/L. Fig. 4 showed the variations of the amount of the adsorbed MB over contact time. It can be seen that a rapid adsorption of MB by CTNTs occurred, with equilibrium reached in approximately 60 min for both concentrations. It was particularly noteworthy that the process showed an extraordinarily fast initial rate of adsorption, which can be verified by the fact that the amount of adsorbed MB onto CTNTs within 5 min almost achieved 90% of that at equilibrium. The fast uptake indicated MB could be easily adsorbed by CTNTs. Additionally, the contact time necessary to reach equilibrium was determined to 4 h in the following equi-

Table 1
BET surface area and porosity of Degussa P25 and CTNTs.

Samples	BET surface area (m^2/g)	Single point total pore volume (cm^3/g)	Average pore diameter (nm)
Degussa P25	46.9	0.18	15.5
CTNTs	157.9	1.32	33.4

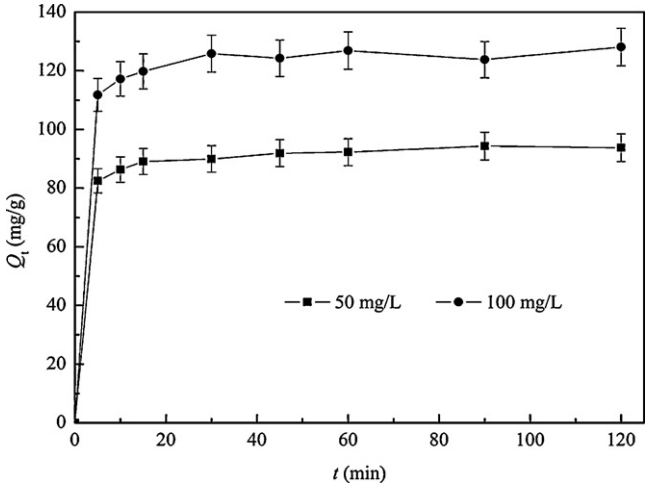

Fig. 4. Effect of contact time on the adsorption of MB onto CTNTs at different initial concentrations. Error bars indicate the standard deviations of three individual experiments.

librium experiment in order to ensure that absolute equilibrium was established.

The adsorption kinetics of MB onto CTNTs was investigated with the aid of two kinetic models, namely the Lagergren pseudo-first-order and pseudo-second-order model. The pseudo-first-order model can be expressed by the following linear form [18]:

$$\ln(Q_e - Q_t) = \ln Q_e - k_1 t \quad (1)$$

where Q_e and Q_t (mg/g) are the amounts of adsorbed MB at equilibrium and at time t, respectively, k_1 (1/min) is pseudo-first-order rate constant, and t (min) is contact time. k_1 can be determined from the slope of the plot of $\ln(Q_e - Q_t)$ versus t.

Another kinetic model is the pseudo-second-order model, which is expressed by [19]

$$\frac{t}{Q_t} = \frac{1}{k_2 {Q_e}^2} + \frac{t}{Q_e} \quad (2)$$

where k_2 (g/(mg min)) is pseudo-second-order rate constant. k_2 is calculated from the intercept of the plot of t/Q_t versus t.

Fig. 5(a) and (b) showed the linear plots of the pseudo-first-order and pseudo-second-order kinetic models at two initial concentrations of 50 and 100 mg/L. The corresponding kinetic parameters obtained from two models (k_1, k_2, Qe1, cal, Qe2, cal, R^2) were listed in Table 2. It can be seen that the fitting of experimental data to the pseudo-first-order model was not so good, with rather low correlation coefficients (R^2), viz. 0.9265 and 0.8400. Accordingly, the experimental data did not obey the pseudo-first-order kinetic model.

Conversely, linear plots of t/Q_t versus t with correlation coefficients higher than 0.999 indicated that the data exhibited a good compliance with pseudo-second-order kinetic equation. It was obvious that the adsorption kinetics of MB onto CTNTs followed the pseudo-second-order kinetic model. It was also found that the pseudo-second-order kinetic model was much more reasonable for MB adsorption process when comparing the calculated and experimental Q_e values. As presented in Table 2, there were

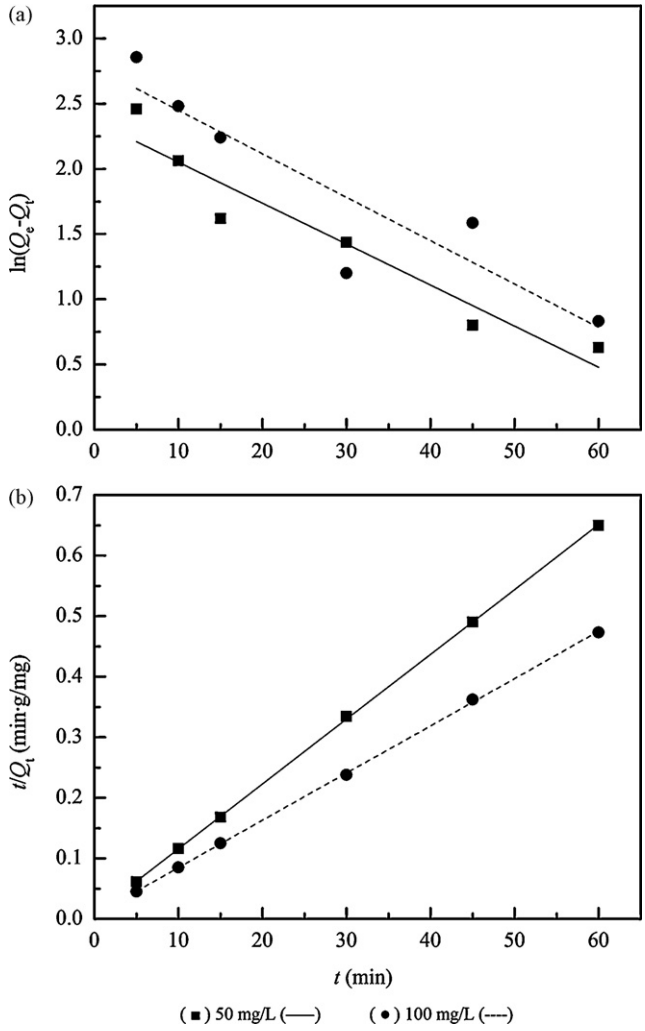

Fig. 5. The linear plot of two kinetic models at different initial concentrations of MB. (a) pseudo-first-order kinetic model and (b) pseudo-second-order kinetic model.

minor deviations between the calculated and experimental Q_e values ($Q_{e2,cal}$ versus $Q_{e,exp}$), while the calculated Q_e values for the pseudo-first-order model ($Q_{e1,cal}$) deviated experimental Q_e values remarkably. The best correlation for the system provided by the pseudo-second-order model suggested that chemical sorption involving valency forces through sharing or exchange of electrons between adsorbent and adsorbate might be significant [20]. A similar adsorption kinetics of MB that well represented by the pseudo-second-order model has been observed onto other adsorbents as well, such as sepiolite [21], natural zeolite [22] and Jordanian diatomite [23].

In order to determine whether intraparticle diffusion was the rate-limiting step in the adsorption process, the Weber's intraparticle diffusion model was introduced to analyze the adsorption kinetic data. This model can be expressed as [24]

$$Q_t = k_{id} t^{0.5} + C \quad (3)$$

Table 2
The determined constants of pseudo-first-order and pseudo-second-order kinetic model with correlation coefficients (R^2) at different initial concentrations.

Initial concentration (mg/L)	Qe, exp (mg/g)	Pseudo-first-order kinetics model			Pseudo-second-order kinetics model		
		k_1 (1/min)	$Q_{e1,cal}$ (mg/g)	R^2	k_2 (g/(mg min))	$Q_{e2,cal}$ (mg/g)	R^2
50	94.15	0.0314	10.65	0.9265	0.0132	93.46	0.9999
100	129.17	0.0333	16.14	0.8400	0.0091	128.21	0.9998

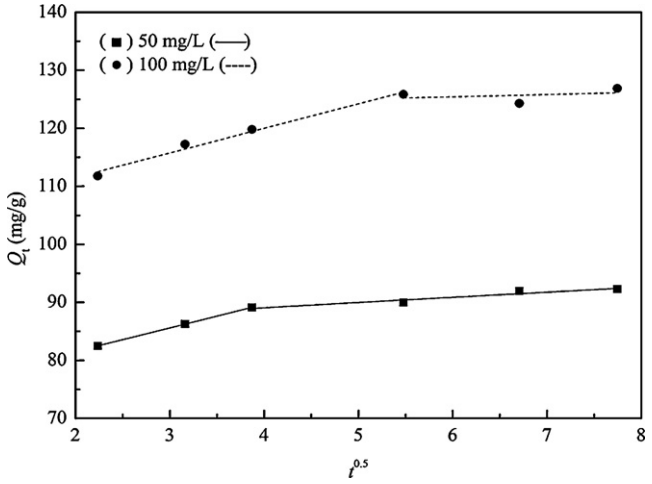

Fig. 6. The linear plot of intraparticle diffusion model at different initial concentrations of MB.

where k_{id} (mg/(g min$^{0.5}$)) is the intraparticle diffusion rate constant and C indicates the boundary layer effect of the adsorption. The plot of Q_t versus $t^{0.5}$ generally consists of the initial portion and the second portion, indicating boundary layer effect and intraparticle diffusion, respectively [25]. A linear plot of the second portion allows to obtain the value of k_{id} and C. The smaller the value of C, the greater the contribution of intraparticle diffusion. If C is equal to zero, the adsorption was solely governed by intraparticle diffusion. However, as illustrated in Fig. 6, the linear plot of the second portion of Q_t versus $t^{0.5}$ did not pass through the origin but the intercept was 85.51 and 123.03 mg/g, respectively. This implied that intraparticle diffusion was not the rate-limiting step, and bulk mass transfer onto the adsorbent described by film diffusion was remarkable in the adsorption process. Similar trend for MB adsorption were also observed onto Neem leaf powder [26] and clay [27], where the overall rate of the dye adsorption process was controlled by both surface adsorption and intraparticle diffusion.

3.4. Adsorption isotherms

The equilibrium adsorption isotherm is indispensable in describing the interaction between pollutant and adsorbent. Fig. 7 depicted the equilibrium adsorption characteristics of MB onto CTNTs at 25 °C. It was observed that the equilibrium adsorption capacity, Q_e, increased with an initial steep rise followed by slight elevation to a more or less plateau promptly along with the increase of equilibrium concentration. The explicit isotherm of L-shape, according to Giles et al. [28], indicated that there is no strong competition between the solvent and the dye to occupy the CTNTs active sites. Moreover, this type of isotherm implies Langmuir-type adsorption between MB and CTNTs molecules. With the increase of initial MB concentration from 25 to 230 mg/L, the amount of the adsorbed MB at equilibrium increased from 47.76 to 135.14 mg/g. The experimental results also showed a decrease of MB removal at equilibrium condition. The removal percentage dropped from 97.96% to 28.36% when the initial concentration rose from 25 to 230 mg/L. This was due to fast saturation on the surface of CTNTs as MB concentration was increased, leading to the decrease of adsorption efficiency. The fact that the removal percentage was higher at lower concentration showed that the available adsorbent surface area was the key factor to achieve high adsorption efficiency.

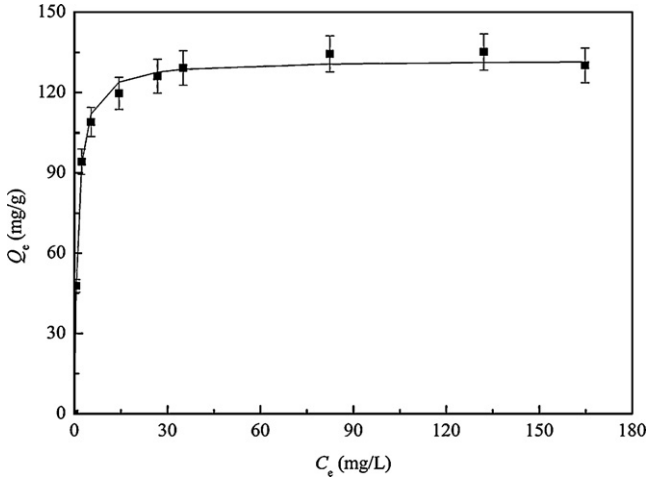

Fig. 7. Adsorption isotherm of MB onto CTNTs at 25 °C. Solid squares correspond to experimental values and solid line corresponds to the fitting curve obtained using a Langmuir equation. Error bars indicate the standard deviations of three individual experiments.

To further describe the equilibrium adsorption isotherm, three isotherm models, i.e. the Langmuir isotherm, the Freundlich isotherm and the Temkin isotherm, were used for test study.

The Langmuir isotherm is based on the assumption that each active site can only hold one adsorbate molecule. The linear equation given by the Langmuir isotherm is expressed as [29]

$$\frac{C_e}{Q_e} = \frac{1}{Q_0 b} + \frac{1}{Q_0} C_e \quad (4)$$

where Q_e (mg/g) and C_e (mg/L) are the amount of adsorbed MB onto CTNTs and MB concentration at equilibrium, respectively, Q_0 (mg/g) is the maximum amount of MB adsorbed per unit mass of CTNTs, and b (L/mg) is a constant related to the adsorption energy. Plotting C_e/Q_e against C_e yields a straight line with the slope $1/Q_0$ and intercept $1/Q_0 b$, then Q_0 and b are determined.

The Freundlich isotherm gives a linear equation as follows [30]:

$$\ln Q_e = \ln K_F + \frac{1}{n} \ln C_e \quad (5)$$

where K_F and n are Freundlich constants. K_F (mg/g (L/mg)$^{1/n}$) indicates relative adsorption capacity of CTNTs, and dimensionless n suggests the favorability of adsorption. A linear plot of $\ln Q_e$ against $\ln C_e$ allows to obtain the values of K_F and n.

The Temkin isotherm can be expressed by [31]

$$Q_e = B \ \ln A + B \ln C_e \quad (6)$$

where $B = RT/b$, b (J/mol) is the Temkin constant related to adsorption heat, T (K) is the absolute temperature, R (8.314 J/(mol K)) is the gas constant, and A (L/g) is the Temkin isotherm constant. B and A can be calculated from the slope and intercept of the plot of Q_e against $\ln C_e$.

The experimental data on MB equilibrium adsorption onto CTNTs were fitted by above-mentioned three isotherm models. The resulted adsorption parameters from fitting were listed in Table 3. It was apparent that the experimental data were fitted much better with the Langmuir isotherm than the other two isotherms, as correlation coefficient R^2 for the Langmuir isotherm was 0.993. The calculated coefficient indicated the monolayer adsorption of MB on CTNTs, with the corresponding monolayer saturated adsorption capacity of 133.33 mg/g at 25 °C according to the fitting result. Table 4 presented saturated adsorption capacities of MB for CTNTs along with some other adsorbents. Clearly, CTNTs exhibited maximum saturated adsorption capacity, which could be ascribed to their large surface area and pore size. The results demonstrated that CTNTs could be employed as promising adsorbents or photocatalysts. The fitting curve was also presented in Fig. 7 by the Langmuir isotherm, which was very close to the experimental data.

Table 3
Isotherm parameters for adsorption of MB onto CTNTs.

Isotherm models	Parameters	
Langmuir	Q_0 (mg/g)	133.33
	b (L/mg)	1.06
	R^2	0.9930
Freundlich	K_F (mg/g (L/mg)$^{1/n}$)	71.23
	n	6.66
	R^2	0.7708
Temkin	A (L/g)	277.27
	B	13.42
	R^2	0.8583

The fact that the Langmuir isotherm fitted the experimental data satisfactorily might be due to uniform nanotubular structure of CTNTs and homogeneous distribution of active sites on the walls. Several authors have also reported this Langmuir-type adsorption behavior of MB dye on other adsorbents. Some of these adsorbents included activated and raw date pits [35], palm kernel fibre [36] and montmorillonite clay [37]. However, Kochkar et al. [38] noted a different behavior for Pd(II) adsorption over titanate nanotubes. They reported that the adsorption curve of Pd(II) on the hydrogenotitanates comprised two different branches, following neither Langmuir nor Freundlich model. This difference could be attributed to different adsorption mechanism for different adsorbates.

The essential characteristic of the Langmuir isotherm can also be evaluated by dimensionless adsorption intensity R_L given by [39]

$$R_L = \frac{1}{1 + bC_0} \tag{7}$$

where C_0 (mg/L) is the initial concentration of MB and b (L/mg) is the Langmuir constant. The parameter R_L indicates the shape of the isotherm to be either unfavorable ($R_L > 1$), linear ($R_L = 1$), favorable ($0 < R_L < 1$) or irreversible ($R_L = 0$). In our experiments the values of R_L at different initial concentration of MB were between 0 and 1, suggesting that the adsorption of MB on the surface of CTNTs was favorable. In addition, the low R_L values (<0.04) implied that the interaction of MB molecules with CTNTs might be relatively strong.

3.5. Adsorption mechanism

As for MB–CTNTs interaction, zeta potential and ATR-FTIR were introduced to gain insight into the adsorption mechanism. Zeta potential of CTNTs was measured in the pH 2.5–11 range with a Nano-ZS90 Zetasizer (Malvern Instruments, England). The suspension concentration of CTNTs was 0.5 g/L, and the temperature was maintained at 25 °C. As presented in Fig. 8, the zeta potential of CTNTs increased with decreasing pH of the suspension, which was in agreement with the study of [40]. It was proposed that hydronium ions derived from lower pH could be adsorbed onto the surface of CTNTs and partially neutralized the negative charge of CTNTs. The negative zeta potentials in the whole pH range indicated that the surface of CTNTs possessed a dominant negative charge.

Table 4
Saturated adsorption capacities of MB for some adsorbents.

Adsorbents	Saturated adsorption capacity (mg/g)	References
Zeolite	16.37	[22]
Neem leaf powder	3.67–19.61	[26]
Activated sewage char	120.00	[32]
NaOH-treated pure kaolin	20.49	[33]
Titania	5.98	[34]
Raw date pits	80.29	[35]
CTNTs	133.33	Present work

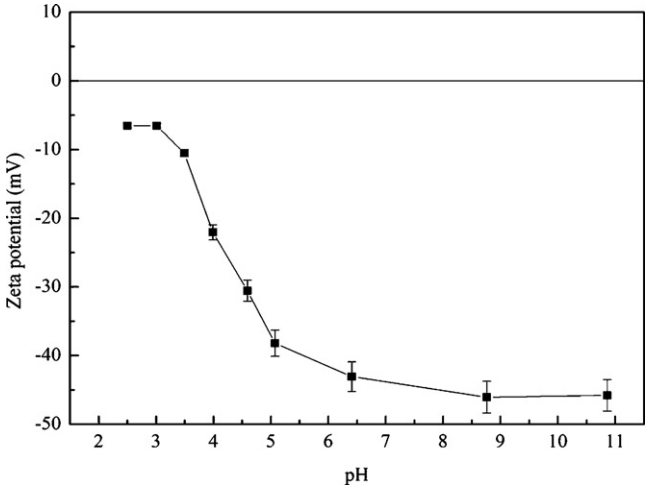

Fig. 8. Variation of zeta potential with pH for CTNTs suspension. Error bars indicate the standard deviations of three individual experiments.

On the other hand, MB was a cation at the solution pH under which the experiments were performed. The cationic MB molecules were readily adsorbed onto negatively charged sites of CTNTs by charge attraction. Therefore, it was concluded that electrostatic attraction might play a major role in the initial bulk diffusion. This was in agreement with previous studies on the adsorption of acid blue 40 onto P25 titania [34] and hexokinase onto silicon wafers [41]. They also indicated that the adsorption was mainly driven by electrostatic forces.

ATR-FTIR spectra of the samples were recorded with a NICOLET iN10 MX spectrometer (Thermo Scientific, USA) equipped with a MCT/A detector and a diamond window, as presented in Fig. 9(a)–(c). All spectra were taken at 64 scans at 4.0 cm^{-1} resolution in the range of 4000–650 cm^{-1}. Fig. 9(a) showed the spectrum of CTNTs. The broad peak at 3347 cm^{-1} corresponded to the stretching vibration of highly OH^- group on the nanotubes. The other two peaks at 1650 and 1363 cm^{-1} might be associated to the Ti–O vibrations. For MB shown in Fig. 9(b), the peak related to the vibration of the aromatic ring at 1600 cm^{-1} was very prominent. Two peaks at 1492 and 1397 cm^{-1} were recognized as the C–N stretching vibrations. The vibrations of the CH_3 group were found at 1356 and 1339 cm^{-1}. Several weak peaks between 1253 and 669 cm^{-1} were ascribed to the C–H in plane and out of plane bending vibrations [42]. The spectrum of MB adsorbed onto CTNTs displayed

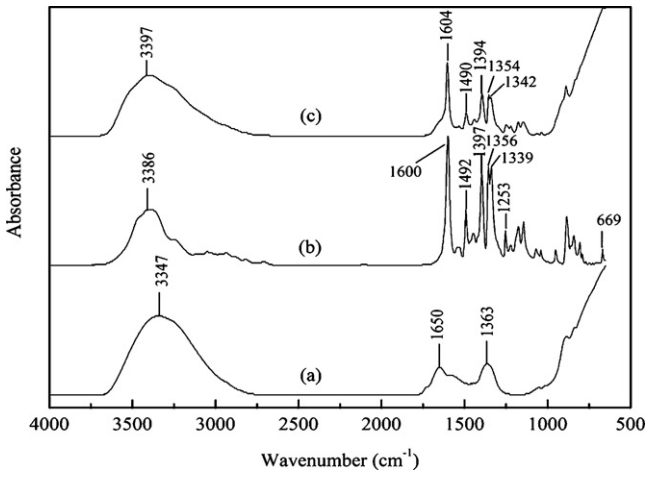

Fig. 9. ATR-FTIR spectra of the samples. (a) CTNTs, (b) MB, and (c) MB adsorbed onto CTNTs.

in Fig. 9(c) preserved the peaks corresponding to MB with the aromatic ring vibration at 1604 cm^{-1}, the C–N stretching vibrations at 1490 and 1394 cm^{-1} and the CH_3 group vibrations at 1354 and 1342 cm^{-1}, reflecting the evidence for the strong interaction between MB and CTNTs, in accordance with the low values of R_L obtained above. Moreover, considering the adsorption process followed the pseudo-second-order kinetics, the sorption process might be mainly controlled by chemical sorption. This was also tested by the necessity to use the Langmuir isotherm model, rather than the Freundlich, to fit the experimental data. Hence, it seemed possible that the formation of MB–CTNTs composite occurred, similar to the reports in Ref. [43], where the MB–TNTs nanocomposite was formed when MB was adsorbed onto TNTs.

4. Conclusions

CTNTs were prepared through an alkaline hydrothermal treatment of TiO_2 (Degussa P25) with 10 M NaOH aqueous solution followed by calcination in the air at 400 °C for 2 h. The morphology and structures of the nanotubes were well-preserved after calcination, keeping a scrolled multi-walled tubular configuration. The present study showed that the CTNTs, with the high surface area of 157.9 m^2/g, had great adsorption capacities of MB. The equilibrium adsorption was attained in nearly 60 min. It was proved that the pseudo-second-order model was most appropriate to describe MB adsorption. Further analysis indicated that the adsorption process was not controlled by intraparticle diffusion. Three adsorption isotherms were introduced to fit the equilibrium data, and the best-fit adsorption isotherm was achieved with the Langmuir but not the Freundlich or Temkin isotherm, indicating monolayer adsorption took place. The highest adsorption capacity was 133.33 mg/g. Based on zeta potential measurement and ATR-FTIR spectra decomposition, the adsorption mechanism can be ascribed to chemical sorption involving the formation of MB–CTNTs nanocomposite, and electrostatic attraction might be predominant in the initial bulk diffusion. Consequently, the CTNTs can be a potential adsorbent due to the high adsorption capacity and a promising catalyst for heterogeneous photocatalysis.

Acknowledgements

The authors would like to acknowledge financial support from the Research Fund for the Doctoral Program of Higher Education (Grant No. 20070001045). Thanks are also to S.F. Weng from College of Chemistry and Molecular Engineering, Peking University for his assistance in ATR-FTIR analysis. The two anonymous reviewers are also gratefully acknowledged for their constructive comments and suggestions.

References

[1] S. Ijima, Helical microtubules of graphitic carbon, Nature 354 (1991) 56–58.
[2] T. Kasuga, M. Hiramatsu, A. Hoson, T. Sekino, K. Niihara, Formation of titanium oxide nanotube, Langmuir 14 (1998) 3160–3163.
[3] Q. Chen, W.Z. Zhou, G.H. Du, L.M. Peng, Trititanate nanotubes made via a single alkali treatment, Adv. Mater. 14 (2002) 1208–1211.
[4] A. Thorne, A. Kruth, D. Tunstall, J.T.S. Irvine, W.Z. Zhou, Formation, structure, and stability of titanate nanotubes and their proton conductivity, J. Phys. Chem. B 109 (2005) 5439–5444.
[5] Y. Guo, N.H. Lee, H.J. Oh, C.R. Yoon, K.S. Park, H.G. Lee, K.S. Lee, S.J. Kim, Structure-tunable synthesis of titanate nanotube thin films via a simple hydrothermal process, Nanotechnology 18 (2007) 295608 (8pp).
[6] J.G. Yu, H.G. Yu, B. Cheng, C. Trapalis, Effects of calcination temperature on the microstructures and photocatalytic activity of titanate nanotubes, J. Mol. Catal. A: Chem. 249 (2006) 135–142.
[7] J.G. Yu, M.H. Zhou, Effects of calcination temperature on microstructures and photocatalytic activity of titanate nanotube films prepared by an EPD method, Nanotechnology 19 (2008) 045606 (6pp).
[8] B. Tryba, A.W. Morawski, M. Inagaki, Application of TiO_2-mounted activated carbon to the removal of phenol from water, Appl. Catal. B 41 (2003) 427–433.
[9] L.X. Zhang, P. Liu, Z.X. Su, A new route for preparation of TiO_2/C hybrids and their photocatalytic properties, J. Mol. Catal. A: Chem. 248 (2006) 189–197.
[10] H. Zhao, S.H. Xu, J.B. Zhong, X.H. Bao, Kinetic study on the photo-catalytic degradation of pyridine in TiO_2 suspension systems, Catal. Today 93–95 (2004) 857–861.
[11] G.W. Wu, A. Koliadima, Y.S. Her, E. Matijevic, Adsorption of dyes on nanosize modified silica particles, J. Colloid Interface Sci. 195 (1997) 222–228.
[12] K. Vinodgopal, D.E. Wynkoop, P.V. Kamat, Environmental photochemistry on semiconductor surfaces: photosensitized degradation of a textile azo dye, acid orange 7, on TiO_2 particles using visible light, Environ. Sci. Technol. 30 (1996) 1660–1666.
[13] X. Ding, X.G. Xu, Q. Chen, L.M. Peng, Preparation and characterization of Fe-incorporated titanate nanotubes, Nanotechnology 17 (2006) 5423–5427.
[14] G.H. Du, Q. Chen, R.C. Che, Z.Y. Yuan, L.M. Peng, Preparation and structure analysis of titanium oxide nanotubes, Appl. Phys. Lett. 79 (2001) 3702–3704.
[15] P. Umek, P. Cevc, A. Jesih, A. Gloter, C.P. Ewels, D. Arcon, Impact of structure and morphology on gas adsorption of titanate-based nanotubes and nanoribbons, Chem. Mater. 17 (2005) 5945–5950.
[16] C.C. Tsai, H.S. Teng, Structural features of nanotubes synthesized from NaOH treatment on TiO_2 with different post-treatments, Chem. Mater. 18 (2006) 367–373.
[17] C.K. Lee, C.C. Wang, M.D. Lyu, L.C. Juang, S.S. Liu, S.H. Hung, Effects of sodium content and calcination temperature on the morphology, structure and photocatalytic activity of nanotubular titanates, J. Colloid Interface Sci. 316 (2007) 562–569.
[18] M. Dogan, M. Alkan, O. Demirbas, Y. Ozdemir, C. Ozmetin, Adsorption kinetics of maxilon blue GRL onto sepiolite from aqueous solutions, Chem. Eng. J. 124 (2006) 89–101.
[19] Y.S. Ho, C.C. Chiang, Sorption studies of acid dye by mixed sorbents, Adsorpt. J. Int. Adsorpt. Soc. 7 (2001) 139–147.
[20] Y.S. Ho, G. McKay, Pseudo-second order model for sorption processes, Process Biochem. 34 (1999) 451–465.
[21] M. Dogan, Y. Ozdemir, M. Alkan, Adsorption kinetics and mechanism of cationic methyl violet and methylene blue dyes onto sepiolite, Dyes Pigm. 75 (2007) 701–713.
[22] R.P. Han, J.J. Zhang, P. Han, Y.F. Wang, Z.H. Zhao, M.S. Tang, Study of equilibrium, kinetic and thermodynamic parameters about methylene blue adsorption onto natural zeolite, Chem. Eng. J. 145 (2009) 496–504.
[23] M.A. Al-Ghouti, M.A.M. Khraisheh, M.N.M. Ahmad, S. Allen, Adsorption behaviour of methylene blue onto Jordanian diatomite: a kinetic study, J. Hazard. Mater. 165 (2009) 589–598.
[24] B.H. Hameed, A.A. Ahmad, N. Aziz, Isotherms, kinetics and thermodynamics of acid dye adsorption on activated palm ash, Chem. Eng. J. 133 (2007) 195–203.
[25] K.G. Bhattacharyya, A. Sharma, Adsorption of Pb(II) from aqueous solution by *Azadirachta indica* (Neem) leaf powder, J. Hazard. Mater. 113 (2004) 99–111.
[26] K.G. Bhattacharyya, A. Sharma, Kinetics and thermodynamics of methylene blue adsorption on Neem (*Azadirachta indica*) leaf powder, Dyes Pigm. 65 (2005) 51–59.
[27] A. Gurses, C. Dogar, M. Yalcin, M. Acikyildiz, R. Bayrak, S. Karaca, The adsorption kinetics of the cationic dye, methylene blue, onto clay, J. Hazard. Mater. 131 (2006) 217–228.
[28] C.H. Giles, T.H. MacEwan, S.N. Makhwa, D. Smith, Studies in adsorption. Part XI. A system of classification of solution adsorption isotherms and its use in diagnosis of adsorption mechanisms and in measurement of specific surface areas of solids, J. Chem. Soc. 56 (1960) 3973–3993.
[29] I. Langmuir, The adsorption of gases on plane surfaces of glass, mica and platinum, J. Am. Chem. Soc. 40 (1918) 1361–1403.
[30] A. Proctor, J.F. ToroVazquez, The Freundlich isotherm in studying adsorption in oil processing, J. Am. Oil Chem. Soc. 73 (1996) 1627–1633.
[31] M.H. Kalavathy, T. Karthikeyan, S. Rajgopal, L.R. Miranda, Kinetic and isotherm studies of Cu(II) adsorption onto H_3PO_4-activated rubber wood sawdust, J. Colloid Interface Sci. 292 (2005) 354–362.
[32] C.I. Sainz-Diaz, A.J. Griffiths, Activated carbon from solid wastes using a pilot-scale batch flaming pyrolyser, Fuel 79 (2000) 1863–1871.
[33] D. Ghosh, K.G. Bhattacharyya, Adsorption of methylene blue on kaolinite, Appl. Clay Sci. 20 (2002) 295–300.
[34] M.L. Fetterolf, H.V. Patel, J.M. Jennings, Adsorption of methylene blue and acid blue 40 on titania from aqueous solution, J. Chem. Eng. Data 48 (2003) 831–835.
[35] F. Banat, S. Al-Asheh, L. Al-Makhadmeh, Evaluation of the use of raw and activated date pits as potential adsorbents for dye containing waters, Process Biochem. 39 (2003) 193–202.
[36] A.E. Ofomaja, Sorption dynamics and isotherm studies of methylene blue uptake on to palm kernel fibre, Chem. Eng. J. 126 (2007) 35–43.
[37] C.A.P. Almeida, N.A. Debacher, A.J. Downs, L. Cottet, C.A.D. Mello, Removal of methylene blue from colored effluents by adsorption on montmorillonite clay, J. Colloid Interface Sci. 332 (2009) 46–53.
[38] H. Kochkar, A. Turki, L. Bergaoui, G. Berhault, A. Ghorbel, Study of Pd(II) adsorption over titanate nanotubes of different diameters, J. Colloid Interface Sci. 331 (2009) 27–31.
[39] A.K. Bhattacharya, S.N. Mandal, S.K. Das, Adsorption of Zn(II) from aqueous solution by using different adsorbents, Chem. Eng. J. 123 (2006) 43–51.
[40] H. Suksri, T. Pongjanyakul, Interaction of nicotine with magnesium aluminum silicate at different pHs: characterization of flocculate size, zeta potential and nicotine adsorption behavior, Colloids Surf. B 65 (2008) 54–60.
[41] S.M. Pancera, H. Gliemann, T. Schimmel, D.F.S. Petri, Adsorption behavior and activity of hexokinase, J. Colloid Interface Sci. 302 (2006) 417–423.

[42] Y.M. Yan, M.N. Zhang, K.P. Gong, L. Su, Z.X. Guo, L.Q. Mao, Adsorption of methylene blue dye onto carbon nanotubes: a route to an electrochemically functional nanostructure and its layer-by-layer assembled nanocomposite, Chem. Mater. 17 (2005) 3457–3463.

[43] M.W. Xiao, L.S. Wang, Y.D. Wu, X.J. Huang, Z. Dang, Electrochemical study of methylene blue/titanate nanotubes nanocomposite and its layer-by-layer assembly multilayer films, J. Solid State Electrochem. 12 (2008) 1159–1166.